IOP Publishing New J. Phys. 25 (2023) 083050 https://doi.org/10.1088/1367-2630/acf1c1

New Journal of Physics
The open access journal at the forefront of physics

Deutsche Physikalische Gesellschaft DPG
IOP Institute of Physics

Published in partnership with: Deutsche Physikalische Gesellschaft and the Institute of Physics

OPEN ACCESS

RECEIVED
12 April 2023

REVISED
1 August 2023

ACCEPTED FOR PUBLICATION
18 August 2023

PUBLISHED
31 August 2023

PAPER

Manipulation of phonon states in ion traps by shortcuts to adiabaticity

Xueying Yang[1,2], Yi Xie[1,2], Jie Zhang[1], Manchao Zhang[1], Chunwang Wu[1], Wei Wu[1], Ting Chen[1,*] and Ping-Xing Chen[1,*]

[1] College of Sciences, National University of Defense Technology, Changsha 410073, People's Republic of China
[2] These authors contributed equally to this work.
[*] Authors to whom any correspondence should be addressed.

E-mail: chenting17@nudt.edu.cn and pxchen@nudt.edu.cn

Keywords: quantum computing, ion trap, Phonon state

Abstract

Shortcuts to adiabaticity (STA) provides the possibility of high accuracy manipulation of phonon states in ion traps. We propose a scheme realized experimentally for manipulating phonon states using STA and confirmed its effectiveness through generating Fock states. Our results show that the duration of the STA manipulation of phonon states is 16 times faster than that of the adiabatic evolution, and the non-resonant excitation can be suppressed by laser bias frequency, which are confirmed by experimental results. Moreover, we also carried out an experimental research on the robustness of STA, showing good robustness respect to the pulse shape deformation, bias noises and stochastic noise. This might lead to a useful step toward realizing fast and noise-resistant quantum manipulation within current experimental capacity.

1. Introduction

Over the past two decades, trapped ions have been successfully used to implement technologies such as quantum computing [1, 2], quantum simulation [3, 4], atomic clocks [5, 6], mass spectrometers [7, 8] and quantum sensors [9]. To experimentally implement scalable quantum computation in trapped ions system, the core issues are how to further improve the manipulation accuracy of ion bits and to increase controllable number of ions [1, 2, 10–14]. One of the more feasible schemes is to expand bits numbers by coupling both the internal states and motional states of ions, which is also called phonon state manipulation in the ion trap [15–19]. Such scheme can be used to create entanglement between ions [20–25], to implement quantum gates [26–29], and to simulate the behavior of complex quantum systems [30–32]. Moreover, phonon modes have been engineered to realize different properties, such as localization, squeezing, and non-classicality [15, 16, 20]. These achievements open up new possibilities for exploring quantum phenomena with phonons, such as quantum metrology, quantum thermodynamics, and quantum error correction [33–35]. Consequently, high accuracy phonon state preparation in ion traps is of great significance since it enables the manipulation of the vibrational states of ions and the control of their interactions with other ions and external fields.

There are two widely used methods for manipulating the phonon states through laser and ion interaction. In one case, there are rectangular pulses that do not depend on time [15], and in the other case, there is the adiabatic method in which the Hamiltonian depends on time explicitly [36]. The duration of the rectangular pulses may be fast. However, to obtain the required accuracy of manipulations, the laser frequency, intensity, and pulse time must be precisely controlled. In addition, the fidelity of phonon states is sensitive to the fluctuation of parameters, leading to poor robustness. On the other hand, adiabatic processes are robust to parameter fluctuations, but require a long evolution time. In real experiments, if the duration of pulse is too long, the scheme will be invalid due to the noises and the decoherence of target state [37].

Combining the advantages of rectangular pulses and adiabatic method, we hope to get a fast and robust scheme, which is easy to implement on the experimental platform. Accelerating the dynamics of adiabatic

passage towards a final outcome is a perfect way to realize fast and robust population transfer. This process can be realized by adding counteradiabatic driving, which is one of the types of shortcuts to adiabaticity (STA) [19, 37–40]. Previously, some theoretical work on realizing STA based on basis vector transformation has been studied in systems such as atoms and NV centers in diamond [41–43]. However, it is difficult to implement counteradiabatic driving in real experiments when Hamiltonian is included in the creation and annihilation operators. Recently, Abah *et al* have theoretically proposed an STA protocol by adding counteradiabatic driving in JC model [38]. With this scheme, the STA Hamiltonian can have a similar form to the original Hamiltonian. This scheme has the characteristics of fast, good robustness and it is theoretically proven to have higher fidelity than previously implemented schemes in ion traps [19].

In this paper, we extend the above theoretical STA protocol from the JC model to the anti-JC model. It can be used in three basic operations of ion trap including carrier, red sideband and blue sideband pulses. Further, we test the effectiveness of such scheme by preparing the Fock state. The effect of non-resonant excitation on fidelity has also been studied. Take advantage of the high robustness of STA, it is found that adding the bias frequency of laser can suppress the non-resonant excitation and improve the fidelity. This scheme also shows higher robustness respect to the pulse shape deformation, bias noises and stochastic noise.

2. Theory model

The interaction of a harmonically trapped ion with a single-mode laser, is described by the Hamiltonian

$$H = \omega_q(t)\sigma_z/2 + \omega_z a^+ a + \frac{\Omega(t)}{2}(\sigma^+ + \sigma)(e^{i(kz-\omega_L t)} + e^{-i(kz-\omega_L t)}), \tag{1}$$

where $\omega_q(t)(\omega_L)$ is the two-level (laser field) frequency and $\Omega(t)$ is the coupling strength between laser field and ion. ω_z is the motional phonon frequency of the ion in harmonic potential. k is the wave number. $\sigma^+(\sigma) = |e\rangle\langle g|(|g\rangle\langle e|)$ is the spin-raising (lowering) operator. The phonon mode is described by the annihilation and creation operators a and a^+ with $[a, a^+] = 1$. Without loss of generality, we assume that the frequency of the two-level system $\omega_q(t)$ and the coupling strength $\Omega(t)$ are time-dependent, while the phonon and laser frequencies remain constants.

Defining the Lamb-Dicke parameter $\eta = k\sqrt{1/(2m\omega_z)}$ and making rotating wave approximation, in the interaction picture the Hamiltonian $U^\dagger(H - i\frac{\partial}{\partial t})U$ takes the form

$$H_I(t) = \frac{\Omega(t)}{2}\left(e^{i\eta(a^+ + a)}\sigma^+ e^{-i\Delta_i t} + H.C.\right) \tag{2}$$

where $\Delta_i = \omega_q(t) - \omega_L$. In the Lamb-Dicke limit, its Taylor expansion can be written as

$$e^{i\eta(a^+ + a)} = 1 + i\eta(a^+ + a) + O(\eta^2), \tag{3}$$

where transitions larger than one phonon will be suppressed. Only carrier transitions($\Delta_i \approx 0$) that do not change the phonon level, and blue($\Delta_i \approx -\omega_z$) or red($\Delta_i \approx \omega_z$) sideband transitions that change a phonon, are possible. For different detuning and picture transformation, the Hamiltonian is written as the following three different forms

$$H_{\text{carrier}} = \frac{1}{2}\left(\omega_q(t) - \omega_L\right)\sigma_z + \frac{\Omega(t)}{2}\sigma_x, \tag{4}$$

$$H_{\text{bsb}}^{\text{aJC}}(t) = \frac{\omega_q(t) - \omega_L}{2}\sigma_z + \omega_z a^+ a + \lambda_b(t)(a^+\sigma^+ + a\sigma^-), \tag{5}$$

$$H_{\text{rsb}}^{\text{JC}}(t) = \frac{\omega_q(t) - \omega_L}{2}\sigma_z + \omega_z a^+ a + \lambda_r(t)(a\sigma^+ + a^+\sigma^-), \tag{6}$$

where the coefficients $\lambda_b = \lambda_r = \eta\Omega(t)$. Rabi frequencies are $\eta\sqrt{n+1}\Omega(t)$ and $\eta\sqrt{n}\Omega(t)$ for the blue and red sideband, respectively. Equations (4)–(6) describe the carrier, blue sideband, and red sideband transitions regions in the ion trap, respectively. It is well known that in real experiments, most bit operations are achieved through the combination of such three types of transitions.

As is well known, adiabatic evolution requires the evolution time be greater than the inverse of the minimum energy gap, and long evolution time leads to more noise dissipation and decoherence. However, this process can be accelerated by introducing an additional counterdiabatic driving into the original Hamiltonian with the following form [44]

$$H_{CD}(t) = i\sum\nolimits_{n,\sigma=\pm}[\partial_t\Phi_{n,\sigma}(t), \Phi_{n,\sigma}(t)], \tag{7}$$

where $\Phi_{n,\sigma}(t) = |n,\sigma(t)\rangle\langle n,\sigma(t)|$ with $|n,\sigma(t)\rangle$ denoting the dressed-atom eigenstates of the original Hamiltonian. Generally speaking, such a additional term is very difficult to realize in real experiment. Abah *et al* have obtained a form similar to the original JC Hamiltonian through ingenious basis vector transformation [38]. Motivated by this idea, we thus optimized three basic operations in the ion trap, including carrier, red and blue sideband pluses. In the case of the carrier transition (equation (4)), the total Hamiltonian $H^{\rm total}_{\rm carrier}(t) = H_{\rm carrier}(t) + H_{\rm CD}(t)$ that ensures perfect transfer at any given time becomes

$$H^{\rm total}_{\rm carrier}(t) = \frac{\omega_q(t)-\omega_L}{2}\sigma_z + \frac{\Omega(t)}{2}\sigma_x + \frac{(\omega_q(t)-\omega_L)\dot{\Omega}(t)-\Omega(t)\dot{\omega}_q(t)}{2\left((\omega_q(t)-\omega_L)^2+\Omega(t)^2\right)}\sigma_y. \tag{8}$$

To circumvent the difficulty in the implementation of additional σ_y-field driving, one make a time-dependent unitary transformation to the total Hamiltonian $H^{\rm total}_{\rm carrier}(t)$ and the appropriate parameters are chosen so that the final Hamiltonian is written as

$$\tilde{H}_{\rm carrier} = \frac{\Omega(t)}{2}\sqrt{1+\frac{\theta_a^2(t)}{\Omega^2(t)}}\sigma_x + \frac{\omega_q(t)-\omega_L}{2}\sigma_z - \frac{\Omega(t)\dot{\theta}_a(t)-\theta_a(t)\dot{\Omega}(t)}{2\left(\theta_a^2(t)+\Omega^2(t)\right)}\sigma_z. \tag{9}$$

where $\theta_a(t) = \frac{\left(\omega_q(t)-\omega_L\right)\dot{\Omega}(t)-\Omega(t)\dot{\omega}_q(t)}{\Omega^2(t)+\left(\omega_q(t)-\omega_L\right)^2}$.

In the case of the blue sideband (equation (5)), in order to ensure that the total Hamiltonian $H^{\rm STA}_{\rm bsb}(t) = H^{\rm aJC}_{\rm bsb}(t) + H_{\rm CD}(t)$ and the original Hamiltonian $H^{\rm aJC}_{\rm bsb}(t)$ have similar forms, we first diagonalize equation (5) in the subspace spanned by $\{|e,n+1\rangle, |g,n\rangle\}$, where $|g\rangle$, $|e\rangle$ as the fundamental and excited state of the two-level system, and $|n\rangle$ is the n-excitation Fock state of the mode. We thus have $H_n(t) = (n+1/2)\omega_z\mathbb{I} + [\delta(t)/2]\bar{\sigma}_z + \lambda(t)\sqrt{n+1}\bar{\sigma}_x$ and the spin-like operators $\bar{\sigma}^- = |g,n\rangle\langle e,n+1|$, $\bar{\sigma}^+ = |e,n+1\rangle\langle g,n|$, $\bar{\sigma}_z = |e,n+1\rangle\langle e,n+1| - |g,n\rangle\langle g,n|$. $\delta(t) = \omega_q(t) - \omega_L + \omega_z$ is the detuning from blue sideband resonance. To ensure that the Hamiltonian $H^{\rm STA}_{\rm bsb}(t)$ equals original equation (5) at the start and end of the protocol, we impose the condition $\dot{\lambda}(0) = \dot{\lambda}(T) = 0$ as well as $\dot{\omega}(0) = \dot{\omega}(T) = 0$. These conditions ensure $H^{\rm STA}_{\rm bsb}(t=0,T) = H^{\rm aJC}_{\rm bsb}(t=0,T)$, which can be recast in finding protocols such that $H_{\rm CD}(t=0,T) = 0$. Then a unitary transformation is performed on $H^{\rm STA}_{\rm bsb}(t)$ so that the new Hamiltonian $\tilde{H}^{\rm aJC}_{\rm bsb}(t) = U^\dagger H^{\rm STA}_{\rm bsb}(t)U$ is similar to the original $H^{\rm aJC}_{\rm bsb}(t)$. This allows us to circumvent the difficulties associated with implementing additional driving. The new Hamiltonian is written as

$$\tilde{H}^{\rm aJC}_{\rm bsb}(t) = \frac{\widetilde{\omega}_q(t)-\omega_L}{2}\sigma_z + \omega_z a^+a + \tilde{\lambda}_b(t)(a^+\sigma^+ + a\sigma^-), \tag{10}$$

where

$$\widetilde{\omega}_q(t) = \omega_q(t) - 2\sqrt{(n+1)}\frac{\lambda_b(t)\dot{\theta}(t)-\theta(t)\dot{\lambda}_b(t)}{\theta^2(t)+\Omega_n^2(t)}, \tag{11}$$

$$\widetilde{\lambda}_b(t) = \left[\lambda_b^2(t)+\theta^2(t)\right]^{1/2}, \tag{12}$$

$$\theta(t) = \frac{\delta(t)\dot{\lambda}_b(t)-\lambda_b(t)\dot{\omega}_q(t)}{\Omega_n^2(t)+\delta^2(t)}, \tag{13}$$

$$\Omega_n(t) = 2\lambda_i(t)\sqrt{n+1}, \tag{14}$$

Note that the driving must also fulfill $\ddot{\lambda}(0) = \ddot{\lambda}(T) = 0$ and $\ddot{\omega}(0) = \ddot{\omega}(T) = 0$ to ensure that $\tilde{H}^{\rm aJC}_{\rm bsb}(t)(t=0,T) = H^{\rm aJC}_{\rm bsb}(t=0,T)$. For that, we consider the protocols $\omega_q(t) = \omega_q(0) + 10\Delta\omega_q s^3 - 15\Delta\omega_q s^4 + 6\Delta\omega_q s^5$, and $\lambda_b(t) = (\lambda_m - \lambda_0)\cos^4[\pi(1+2s)/2] + \lambda_0$, with $s = t/T$, $\Delta\omega_q = \omega_q(T) - \omega_q(0)$, and λ_0 is the initial coupling constant, while λ_m denotes its maximum value. As for a Landau-Zener problem, a population transfer between $\{|e,n+1\rangle$ and $|g,n\rangle\}$ requires that $\omega_q(t)$ changes its sign during the evolution while $\lambda_b(t) \neq 0$ for some t with $\lambda(0) = \lambda(T) = 0$, which also applies to the modified frequencies.

In the case of the red sideband (equation (6)), The local counterdiabatic Hamiltonian $\tilde{H}^{\rm JC}_{\rm rsb}(t) = \frac{\widetilde{\omega}_q(t)-\omega_L}{2}\sigma_z + \omega_z a^+a + \tilde{\lambda}_r(t)(a\sigma^+ + a^+\sigma^-)$ has a similar derivation process with $\tilde{H}^{\rm JC}_{\rm bsb}(t)$, except that $\delta(t) = \omega_q(t) - \omega_L - \omega_z$ and all $\tilde{\lambda}_b(t)$ should be replaced by $\tilde{\lambda}_r(t)$.

We now consider the effectiveness of our STA scheme through the preparation of Fock state. The Fock state is deterministically prepared by n laser pulse trains, each contains carrier transition with π pulses and the blue/red sideband transition. Since carrier transition is usually very fast in experiments, STA is only

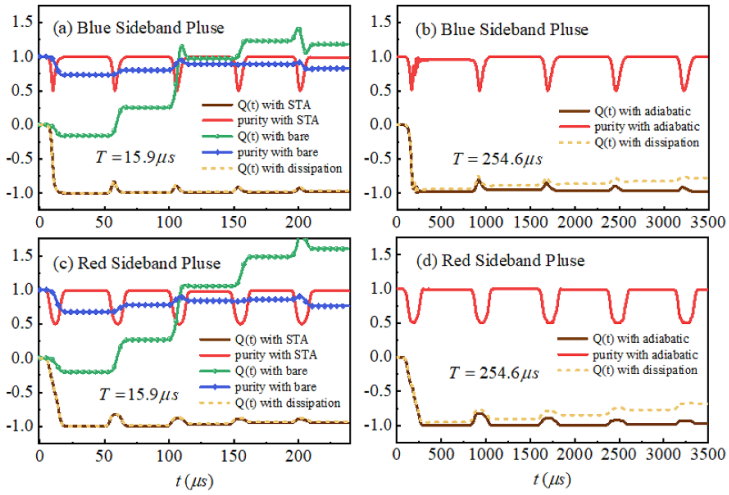

Figure 1. Scheme for the generation of Fock states from $n=0$ to 5. (a) Preparing a Fock state using alternate blue sideband and carrier π pulses. The evolution of Mandel parameter $Q(t)$ and purity $p(t)$ of Fock state prepared by STA and adiabatic method, respectively, and $T=15.9\,\mu$s. (b) Preparing the same fidelity of Fock state as STA in (a) by using the original Hamiltonian, but with larger $T=254.6\,\mu$s. (c) and (d) are the same as (a) and (b), respectively, except that the red sideband is replaced by the blue sideband. Other parameters are $\omega_q(0)=3\omega/2$, $\omega_q(T)=\omega/2$, $\lambda_0=0$, $\lambda_m=\omega/4$, $\omega=2\pi\times 50\,$kHz.

applied for accelerating the sideband transition. Figure 1 shows the evolution of the Mandel parameter $Q(t)=\frac{\langle n^2(t)\rangle-\langle n(t)\rangle^2}{\langle n(t)\rangle}-1$, which accounts for the nonclassicality of the resulting state, and the purity $p(t)=\mathrm{Tr}_b[\rho_s^2(t)]$ of the reduced two-level state $\rho_s(t)=\mathrm{Tr}_b[\rho(t)]$. $\rho(t)$ is density matrix of the total system and $\mathrm{Tr}_b[.]$ denoting the trace over the phonon mode. Figure 1(a) shows the evolution of $Q(t)$ and $p(t)$ from $n=0$ to 5 for STA and bare Hamiltonian, respectively. It is found that for same duration $T=15.9\ \mu$s, the Mandel parameter $Q(t)$ unveils the sub-Poissonian behavior of the boson statistics (i.e. $Q(t)<0$). It is defined as the normalized variance of the phonon distribution. For a perfect population transfer, the minimal value $Q(t)=-1$ is obtained from each STA+π cycle. The closer the $Q(t)$ value is to -1, the higher the fidelity of the Fock state. The purity $p(t)$ almost keep 1 for STA. Compared to STA case, the system without STA finally evolves into the undesired target state (see the green and blue lines). Until the duration increases to $T=254.6\ \mu$s, such a system can achieve the same effect as STA, as show in figure 1(b). In addition, we compute the time evolution of the system according to a Lindblad master equation that accounts for experimental imperfections resulting in heating and decoherence of the motional modes:

$$\begin{aligned}\dot{\hat{\rho}}(t)=&-i[\hat{H},\hat{\rho}(t)]\\&-\Gamma\left[\hat{\rho}(t)\hat{a}^\dagger\hat{a}\hat{a}^\dagger\hat{a}-2\hat{a}^\dagger\hat{a}\hat{\rho}(t)\hat{a}^\dagger\hat{a}+\hat{a}^\dagger\hat{a}\hat{a}^\dagger\hat{a}\hat{\rho}(t)\right]\\&-\frac{\gamma}{2}n_{\mathrm{th}}\left[\hat{a}\hat{a}^\dagger\hat{\rho}(t)-2\hat{a}^\dagger\hat{\rho}(t)\hat{a}+\hat{\rho}(t)\hat{a}\hat{a}^\dagger\right]\\&-\frac{\gamma}{2}(n_{\mathrm{th}}+1)\left[\hat{a}^\dagger\hat{a}\hat{\rho}(t)-2\hat{a}\hat{\rho}(t)\hat{a}^\dagger+\hat{\rho}(t)\hat{a}^\dagger\hat{a}\right].\end{aligned}\tag{15}$$

Here, Γ is the decoherence parameter, which we set to be $\Gamma=(1/\tau)$, with $\tau=2.5$ ms. γ is the coupling strength between the ion motion and the thermal reservoir, and n_{th} is the average phonon number when the system is in equilibrium with the environment. In our model, the effective temperature of the thermal reservoir is infinite, which makes n_{th} extremely large and $\gamma n_{\mathrm{th}}\approx\gamma\,(n_{\mathrm{th}}+1)$. It is natural to define the heating rate as γn_{th}, which is measured as $60\pm3.02\ quanta\,s^{-1}$ in our system. Due to the addition of dissipation to the case of STA, the Mandel parameter $Q(t)$ decreases by 2% for $n=5$, from -0.98 to -0.96, as shown in figure 1(a) with the solid brown line and the dashed yellow line. Figure 1(b) illustrates that the $Q(t)$ decreases by 20%, from -0.97 to -0.77, after adding dissipation to adiabatic evolution. Thus, STA manipulation of phonon states is 16 times faster than adiabatic evolution, and STA has a significant effect on dissipation as well.

It is worth noting that we have calculated the quantum speed limit time of Mandelstam and Tamm, $\tau=\pi/2\Delta H$, where ΔH is the variance of the Hamiltonian of the quantum system. Since the Hamiltonian is time-dependent according to equation (10), we average the quantum velocity limit time τ to obtain $\bar{\tau}=\int_0^T\tau(t)\mathrm{d}t/T$. When the actual evolutionary period $T=15.9\,\mu$s , the average limit time $\bar{\tau}=4.8\,\mu$s. As a result of STA's acceleration, it does not exceed the quantum speed limit time. We note that figures 1(a)

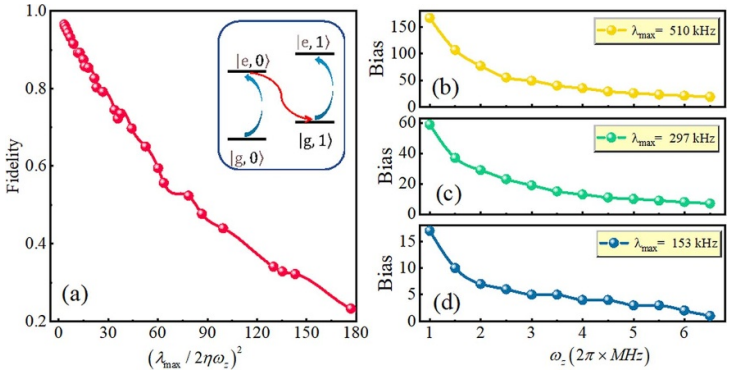

Figure 2. (a) The fidelity as a function of the strength of non-resonance excitation. (b) For the fidelity to more than 0.95, appropriate bias frequency is required for different ion motional frequencies, and for fixed maximum Rabi frequency. The maximum Rabi frequency λ_{max} of laser is 510 kHz, 297 kHz, 153 kHz for (b), (c), and (d), respectively.

and (b) are for case of blue sideband, while figures 1(c) and (d) are for the red sideband one, which exhibits qualitatively similar behavior. Consequently, in what follows we only focus on the region of red sideband.

Up to now, the coupling strength of non-resonant processes are assumed to be smaller than the detuning, and thus the effects of a variety of non-resonant excitations are not included. However, in realistic experiments the non-resonant excitations can severely degrade the fidelity of the final state, especially for the case where laser excites transition on a sideband and the non-resonant carrier transition should be taken into account. For example, if the transition $|e,0\rangle \leftrightarrow |g,1\rangle$ is driving from pure initially $|e,0\rangle$, then the populations of $|g,0\rangle$ and $|e,1\rangle$ are proportional to the populations of $|e,0\rangle$ and $|g,1\rangle$, respectively, with the proportionality factor given by $[\lambda(t)/2\eta\omega_z]^2$.

Figure 2(a) shows the variation of fidelity as a functions of the strength of non-resonance excitation for the preparation of Fock states from $|e,0\rangle$ to $|g,1\rangle$. It is easy to see that the fidelity of the system shows strong dependence on both Rabi frequencies λ_{max} and motional frequencies ω_z. Take advantage of the high robustness of STA, we can change the laser frequency to suppress non-resonant excitation with fixed motional frequency ω_z and laser power. To improve the fidelity to more than 0.95, we should add appropriate bias frequency, as shown in figures 2(b)–(d) for different ion motional frequencies ω_z, but for fixed maximum Rabi frequency λ_{max}. The stronger laser power, the larger bias frequency is required. The smaller motional frequency, the larger bias frequency is required with fixed laser power.

3. Experimental results

3.1. Experimental setup and sequence

We now discuss the experiment scheme and the related sequence. We employ the axial mode of a single trapped $^{40}Ca^+$ ion in a harmonic potential with the frequency of $\omega_z = 2\pi \times 1.3$ MHz to prepare Fock states. A Zeeman splitting of about 8.8 MHz is created by a magnetic field in $D_{5/2}$, and the sublevels $^2S_{1/2}(m_j = -1/2)$ and $^2D_{5/2}(m_j = -1/2)$ are chosen as the qubit states $|g\rangle$ and $|e\rangle$, respectively, as shown in figure 3(a). Initially, the ion is prepared at state $|g,0\rangle$ (namely the state $|g\rangle$ with 0 phonon number) by Doppler cooling, EIT cooling, sideband cooling. State manipulation is achieved by 729 nm laser pulses from a stabilized Ti-sapphire laser with linewidth about 20 Hz. The laser beam is sent through acoustooptic modulators (AOM) and then focused to the position of the ion. AOM is used to control the frequency and amplitude of the laser beam. Quantum operations and laser beam modulations are realized by transmitting RF signals generated by signal generator or arbitrary waveform generator(AWG) to AOM. By scanning the Rabi oscillation, a relationship between the amplitude of the AWG and the Rabi frequency is obtained, and the AC stark shift needs to be compensated for the waveform's pre-calibration. The actual waveform of AWG is generated based on the theoretically calculated Rabi frequency and detuning over time. It is necessary that the input waveform sample at a rate greater than or equal to the sample rate required by the AWG. Figures 3(b) and (c) show the actual shape of the waveform without and with the STA scheme. The final state is detected by a laser pulse of 397 nm.

For trapped ions system, Fock states can be generated by pseudo-spin phonon coupling, which usually need fast and accurate control of both the internal and the motional states. The laser timing sequence of Fock state generation is shown at the top of figure 4. We start from $|e,0\rangle$, and then followed by a series of alternating red sideband transitions ($|e,n\rangle \leftrightarrow |g,n+1\rangle$) and carrier transitions ($|g,n\rangle \leftrightarrow |e,n\rangle$), which are marked by the red and grey squares, respectively. Figure 4(a) shows the time evolution of population of $|e\rangle$ in

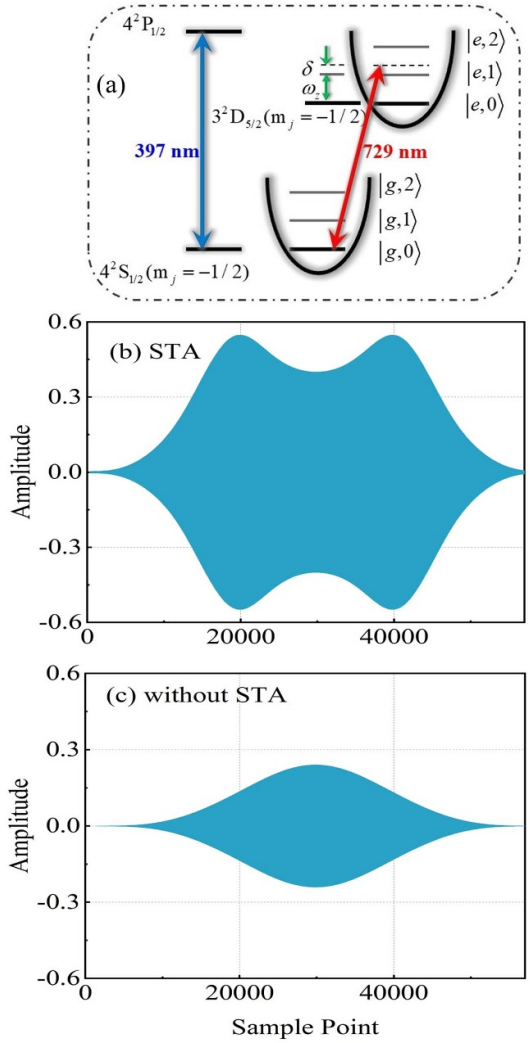

Figure 3. (a) Energy level structure of $^{40}Ca^{+}$ ion and relevant laser wavelengths. (b) Waveform of AWG with STA protocol. (c) Waveform of AWG without STA.

the absence of bias during the pulse sequence, and the change of phonon number is marked at the top of figure 4(a).

The first red sideband transition did not completely flip the internal state of ions. This will directly reduce the fidelity of phonon state preparation. As discussed before, infidelity is mainly caused by non resonant excitation and proportional to laser power. The first red sideband transition requires the highest laser power and suffers most affection by non-resonant excitation. However, when the bias frequency increases to 11 kHz, the fidelity of internal state after the first red sideband is significantly improved, as show in figure 4(b). This is consistent with our theoretical prediction.

After the target state has been prepared to $|e,5\rangle$, we measure the final distribution of phonon number by driving the blue sideband transitions and fitting the $|e,n\rangle$ state population with the under-determined parameters as the Fock state population P_n [45]. Each measurement is repeated 1500 times to ensure the reliability of our results. We obtain the phonon number distribution by fitting blue sideband time evolution with bias frequency 0 kHz and 11 kHz, respectively, as shown in figures 4(c) and (d). It is found that the fidelity is increased from 0.45 to 0.864.

Last but not least, we should make a balance between the speed and fidelity when we use the STA protocol. To avoid decoherence during state transitions, short pulses are preferred, but shorter pulse periods mean stronger laser power and higher non resonant transitions, which lead to lower fidelity. Figure 4(e) shows the optimization fidelity of our experimental Fock states from $n=0$ to 8. Furthermore, the fidelity can also be influenced by the heating rate. In our current experimental setup, the heating rate has been quantified as $60 \pm 3.02\ quanta\,s^{-1}$ while the maximum operational duration is approximately 400 μs. By utilizing the heating rate obtained from the experiment, the corresponding increase in phonon number is calculated to be 0.024 ± 0.0012.

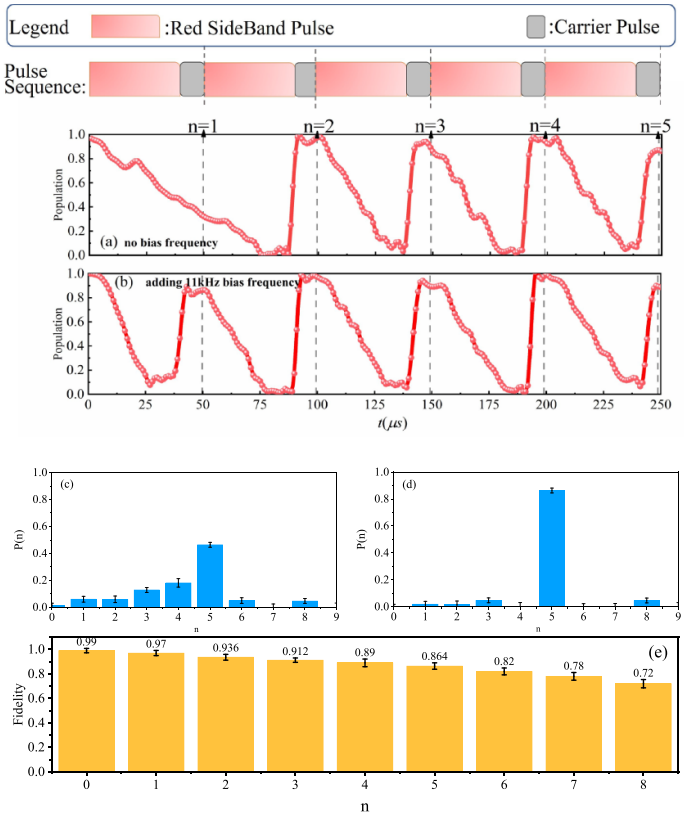

Figure 4. (a) The population of $|e,n\rangle$ vs time from $|e,0\rangle$ to $|e,5\rangle$ with laser bias frequency 0 kHz and 11 kHz in (a), (b) respectively. Evolutionary periods $T = 47.74\,\mu$s. The phonon number distribution under $n = 5$ with laser bias frequency 0 kHz and 11 kHz in (c), (d) respectively. (e) Fidelity of Fock states preparation for the phonon number from 0 to 8 with STA in appropriate bias frequency.

3.2. The Robustness of the system

3.2.1. The effect of the pulse shape deformation

We next consider the robustness of our STA protocol to the pulse shape of the 729 nm laser. Due to the Gaussian shape of the laser beam, atoms at different positions are subjected to different Rabi frequencies. Despite prior calibration, strict precision cannot be guaranteed due to power dithering. In addition, it is difficult to exactly solve the shape of pulse from equations (11) and (12). To avoid long-time drift of laser frequency, numerical simulation is required. We investigate the flexibility of the performance to imperfect pulse implementations. To do this, we approximate the actual form of the pulse $\widetilde{\lambda}_r(t)$ and $\widetilde{\delta}_r(t) = \tilde{\omega}_q(t) - \omega_L - \omega_z$ with N_F Fourier modes, namely, via

$$\widetilde{x}_F(t) = \sum_{k=0}^{N_F} c_k \cos(k\omega_F t) + s_k \sin(k\omega_F t), \tag{16}$$

where $\widetilde{x}_F(t)$ denoting the approximation of $\widetilde{x}(t)$ with $\tilde{x} \in \{\widetilde{\lambda}_r(t), \widetilde{\delta}_r(t)\}$ using N_F modes.

In figures 5(a) and (b), we show the approximate profiles with different N_F for the $n = 0$ subspace. Note that for $N_F = 8$, the Fourier mode agrees with exact solution. Five different Fourier modes are implemented experimentally for transition $|e,0\rangle \leftrightarrow |g,1\rangle$ and shown in figure 5. The influence on the fidelity was investigated for approximation made on frequency only, power only and both of the two. The final results are shown in table 1.

Under the theoretical calculation [38], Abah *et al* have confirmed that increasing N_F the infidelity becomes arbitrarily small. When the evolution period is $\omega T = 6$, the infidelity is within 10^{-4} even if $N_F = 1$. The fidelities in table 1 have not changed significantly. The experimental results are in agreement with the theory one. The different between numerical and experimental infidelities mainly comes from the non-resonant transitions and states measurement. The first column of table 1 is the results that only the laser power is approximated. For $N_F = 1$ and 2, the fidelities are slightly higher than those for $N_F = 4$ and 8. This can be explained as follows. Referring to figure 5(a), for $N_F = 1$ and 2, the waveforms are single peaks, while double peaks for $N_F = 4$ and 8. The average power of single peak is weaker than that of the double peak. In other words, for $N_F = 1$ and 2, the non-resonance excitation caused by the strong laser power is less.

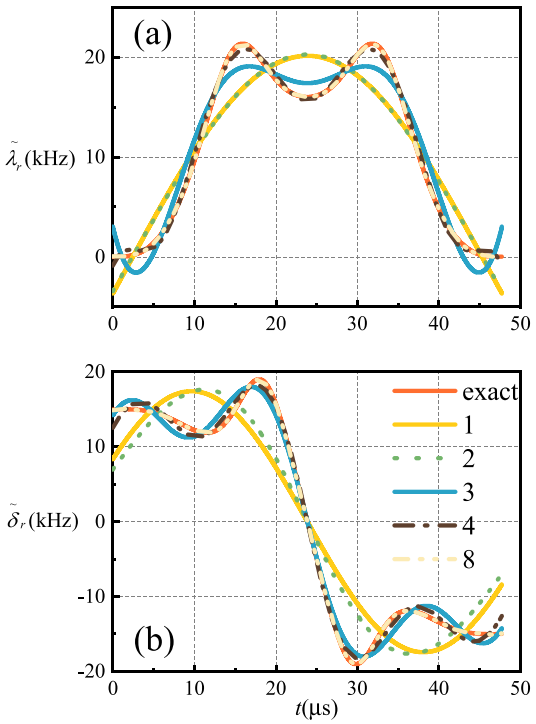

Figure 5. Parameter Fourier expansion of different series, $\widetilde{\lambda}_r$ and $\widetilde{\delta}_r$ in (a) and (b), respectively, plotted with red lines for exact pulse shape. Others correspond to the approximated pulses using N_F Fourier modes, as indicated in legend.

Table 1. The fidelities of Fock states with different N_F Fourier modes.

N_F	$\widetilde{\lambda}_r$	$\widetilde{\delta}_r$	$\widetilde{\lambda}_r+\widetilde{\delta}_r$
1	0.973 ± 0.021	0.951 ± 0.045	0.945 ± 0.022
2	0.972 ± 0.018	0.951 ± 0.017	0.949 ± 0.027
3	0.970 ± 0.014	0.959 ± 0.031	0.960 ± 0.040
4	0.961 ± 0.034	0.961 ± 0.034	0.958 ± 0.011
8	0.965 ± 0.012	0.965 ± 0.021	0.962 ± 0.025

This confirms once again that for a small number of operations, the fidelity depends mainly on the non-resonant excitation. The second and third columns show that fidelity becomes higher with increasing of N_F. The robustness of STA protocol performance is strongly good against imperfect pulse implementation.

3.2.2. The effect of bias noise

Pulse shaping protocols are also commonly used in experiments to suppress non-resonant excitation, where the pulse shape of the 729 nm laser beam is changed from the ordinary rectangular form [18]

$$E(t) = A\sin[(\omega_0 - \delta_{AC})t + \varphi], \tag{17}$$

to a sine-shaped form

$$E(t) = \frac{\pi A}{2}\sin\left[\frac{\pi t}{T}\right] \times \sin\left[\omega_0 t + \frac{\pi^2 \delta_{AC}}{8}\left(2\pi t - T\sin\left[\frac{2\pi t}{T}\right]\right) + \varphi\right], \tag{18}$$

where A is the amplitude factor, ω_0 and φ are the resonance frequency and phase, respectively, δ_{AC} is the compensation for the AC-Stark shift effect and T is the duration of the pulse.

In order to compare the robustness of the two schemes to bias noises, we artificially introduce bias noises. Figure 6 shows the influence of bias noises on the fidelity in the STA and pulse shaping schemes. Δ indicates how many the laser frequency drifts relative to δ. Experimentally, the value of Δ is changed by adjusting the driving frequency of AOM. The transition is between $|e,0\rangle$ and $|g,1\rangle$. If the fidelity above 0.8 is set as acceptable, STA can endure laser detuned by 9 kHz but pulse shaping only 5 kHz. STA shows better robustness to bias noises.

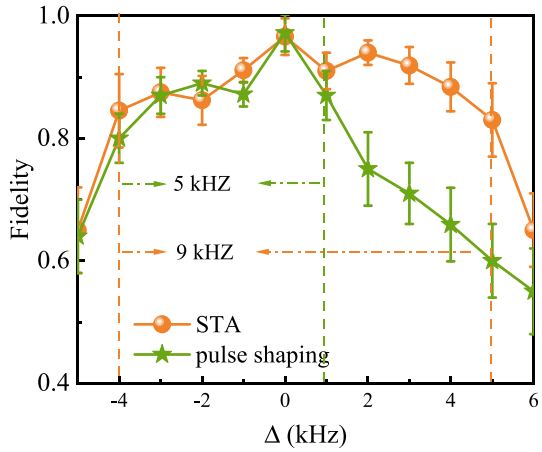

Figure 6. The fidelities of the transition $|e,0\rangle \leftrightarrow |g,1\rangle$ at different center frequencies for shortcuts to adiabaticity and pulse shaping schemes.

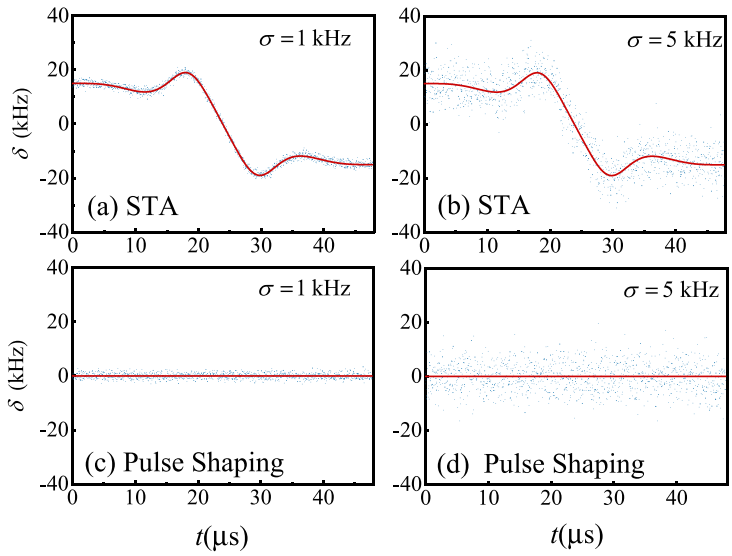

Figure 7. Detuning frequencies with stochastic noise in two protocols.

3.2.3. The effect of stochastic noise

The third type of noise is the stochastic one, which mainly refers to magnetic field noise caused by environment and short-time jitter of laser frequency and power. In the experiment, stochastic noise is uncontrollable. In order to compare the robustness of the two schemes to stochastic noises, we artificially introduce stochastic noises.

Since the Rabi frequency is controlled by the 729 nm laser power, we add Gaussian $N(\mu,\sigma^2)$ random noises at Rabi frequency using an AWG and an AOM. We study the influence of stochastic laser frequency noise on the fidelity. The laser phase noise is uniform and independent on frequency. Thus Gaussian $N(\mu,\sigma^2)$ random noise for detuning frequency use $\sigma = 1$ kHz, 5 kHz and 10 kHz respectively. Figure 7 shows the time dependent frequency detuning with stochastic noise for $\sigma = 1$ kHz, 5 kHz, respectively. The red line is the exact solution, and the blue dots are the parameters with stochastic noise. The transition is between $|e,0\rangle$ and $|g,1\rangle$ in π pulses time. Figures 7(a) and (b) are for STA protocol and (c) and (d) are for pulse shaping protocol.

The fidelities with different stochastic laser frequency noise are shown in table 2. When there is no extra noises ($\sigma = 0$ kHz), the fidelity of STA protocol is about 0.971 and that of pulse shaping is about 0.976. When adding the Gaussian $N(\mu,\sigma^2)$ stochastic noises with $\sigma = 1$ kHz, the fidelity of STA protocol is almost unchanged but that of pulse shaping decreases 2.6%. As the noise increases, the fidelities of both schemes decrease from table 2. But the fidelity of STA protocol is slightly higher and decreases slower than that of pulse shaping. It shows STA protocol has better robustness to stochastic frequency noise.

Table 2. The fidelities of Fock states with different stochastic noise for detuning frequencies.

σ	0 kHz	1 kHz	5 kHz	10 kHz
STA	0.971 ± 0.011	0.970 ± 0.013	0.923 ± 0.024	0.894 ± 0.017
Pulse shaping	0.976 ± 0.013	0.950 ± 0.015	0.903 ± 0.020	0.862 ± 0.011

A key reason why the STA exhibits good robustness in the presence of additional bias noise as well as random noise is due to its counterdiabatic driving method. As the basic idea of counterdiabatic drive, an auxiliary term is required in order to make the dynamics follow exactly the approximate adiabatic evolution driven by original Hamiltonian. An approximate adiabatic evolution is robust to parameter changes since it follows the eigenstates of the original Hamiltonian.

4. Conclusion

In summary, we have proposed a scheme realized experimentally by using STA, which can be used to accelerate the duration of the red/blue sideband. Based on the real experimental environment, our numerical simulation shows the destruction of fidelity is induced by different non-resonant excitations. However, it is found that such non-resonant excitations can be suppressed by adding the bias frequency of laser and the fidelity of phonon states can also be improved, which are also confirmed by our experimental results. Finally, the STA shows good robustness respect to the pulse shape deformation, bias noises and stochastic noise. These conclusions will provide important technical reference to manipulate the phonon states in trapped ion system.

Data availability statement

All data that support the findings of this study are included within the article (and any supplementary files).

Acknowledgments

This work is supported by the National Natural Science Foundation of China under Grant Nos. 12074433, 12004430, 12174447 and 12174448.

References

[1] Blatt R and Roos C F 2012 *Nat. Phys.* **8** 277
[2] Häffner H, Roos C F and Blatt R 2008 *Phys. Rep.* **469** 155
[3] Friedenauer A, Schmitz H, Glueckert J T, Porras D and Schaetz T 2008 *Nat. Phys.* **4** 757
[4] Islam R, Senko C, Campbell W C, Korenblit S, Smith J, Lee A, Edwards E E, Wang S, Freericks J K and Monroe C 2013 *Science* **340** 583
[5] Leibfried D, Blatt R, Monroe C and Wineland D J 2003 *Nature* **422** 412
[6] Katori H 2011 *Nat. Photon.* **5** 203
[7] Guo Q, Gao L, Zhai Y and Xu W 2018 *Chin. Chem. Lett.* **29** 1578
[8] Schwartz J C, Senko M W and Syka J E 2002 *J. Am. Soc. Mass Spectrom.* **13** 659
[9] Reiter F, Sørensen A S, Zoller P and Muschik C A 2017 *Nat. Commun.* **8** 1822
[10] Benhelm J, Kirchmair G, Roos C F and Blatt R 2008 *Nat. Phys.* **4** 463
[11] Cirac J I and Zoller P 2000 *Nature* **404** 579
[12] Hensinger W K 2011 *Nature* **476** 155
[13] Monz T, Kim K, Hänsel W, Riebe M, Villar A S, Schindler P, Chwalla M, Hennrich M and Blatt R 2009 *Phys. Rev. Lett.* **102** 040501
[14] Kielpinski D, Monroe C and Wineland D J 2002 *Nature* **417** 709
[15] Zhu S-L, Monroe C and Duan L-M 2006 *Phys. Rev. Lett.* **97** 050505
[16] An S, Zhang J-N, Um M, Lv D, Lu Y, Zhang J, Yin Z-Q, Quan H T and Kim K 2015 *Nat. Phys.* **11** 193
[17] Vahala K, Herrmann M, Knünz S, Batteiger V, Saathoff G, Hänsch T W and Udem T 2009 *Nat. Phys.* **5** 682
[18] Zhang J, Um M, Lv D, Zhang J-N, Duan L-M and Kim K 2018 *Phys. Rev. Lett.* **121** 160502
[19] Um M, Zhang J, Lv D, Lu Y, An S, Zhang J-N, Nha H, Kim M S and Kim K 2016 *Nat. Commun.* **7** 11410
[20] Krutyanskiy V *et al* 2023 *Phys. Rev. Lett.* **130** 050803
[21] Nicacio F, Furuya K and Semi ao F L 2013 *Phys. Rev.* A **88** 022330
[22] Casabone B, Stute A, Friebe K, Brandstätter B, Schüppert K, Blatt R and Northup T E 2013 *Phys. Rev. Lett.* **111** 100505
[23] Härkönen K, Plastina F and Maniscalco S 2009 *Phys. Rev.* A **80** 033841
[24] Bentley C D B, Carvalho A R R, Kielpinski D and Hope J J 2014 *Phys. Rev. Lett.* **113** 040501
[25] Ruster T, Kaufmann H, Luda M A, Kaushal V, Schmiegelow C T, Schmidt-Kaler F and Poschinger U G 2017 *Phys. Rev.* X **7** 031050
[26] Manovitz T, Shapira Y, Gazit L, Akerman N and Ozeri R 2022 *PRX Quantum* **3** 010347
[27] de Clercq L E, Lo H-Y, Marinelli M, Nadlinger D, Oswald R, Negnevitsky V, Kienzler D, Keitch B and Home J P 2016 *Phys. Rev. Lett.* **116** 080502
[28] Ballance C J, Harty T P, Linke N M, Sepiol M A and Lucas D M 2016 *Phys. Rev. Lett.* **117** 060504

[29] Olsacher T, Postler L, Schindler P, Monz T, Zoller P and Sieberer L M 2020 *PRX Quantum* **1** 020316
[30] Xu Y-Z, Zhao W-D, Hou Y-H, Mei Q-X, Ma J-Y, Wang J, He L, Zhou Z-C, Wu Y-K and Duan L-M 2020 *Phys. Rev.* A **102** 063121
[31] Lin G-D, Monroe C and Duan L-M 2011 *Phys. Rev. Lett.* **106** 230402
[32] Li B-W, Mei Q-X, Wu Y-K, Cai M-L, Wang Y, Yao L, Zhou Z-C and Duan L-M 2022 *Phys. Rev. Lett.* **129** 140501
[33] Zhang J-W *et al* 2022 *Nat. Commun.* **13** 6225
[34] Postler L *et al* 2022 *Nature* **605** 675
[35] Yang H-X, Ma J-Y, Wu Y-K, Wang Y, Cao M-M, Guo W-X, Huang Y-Y, Feng L, Zhou Z-C and Duan L-M 2022 *Nat. Phys.* **18** 1058
[36] Yanagimoto R, Ng E, Onodera T and Mabuchi H 2019 *Phys. Rev.* A **100** 033822
[37] Guéry-Odelin D, Ruschhaupt A, Kiely A, Torrontegui E, Martínez-Garaot S and Muga J G 2019 *Rev. Mod. Phys.* **91** 045001
[38] Abah O, Puebla R and Paternostro M 2020 *Phys. Rev. Lett.* **124** 180401
[39] Schaff J-F, Capuzzi P, Labeyrie G and Vignolo P 2011 *New J. Phys.* **13** 113017
[40] Roos C 2012 *Physics* **5** 94
[41] Lin J-Z 2018 *Ann. Phys., Lpz.* **530** 1700456
[42] Huang B-H, Kang Y-H, Chen Y-H, Wu Q-C, Song J and Xia Y 2017 *Phys. Rev.* A **96** 022314
[43] Baksic A, Ribeiro H and Clerk A A 2016 *Phys. Rev. Lett.* **116** 230503
[44] Berry M V 2009 *J. Phys. A: Math. Theor.* **42** 365303
[45] Bertet P, Osnaghi S, Milman P, Auffeves A, Maioli P, Brune M, Raimond J M and Haroche S 2002 *Phys. Rev. Lett.* **88** 143601